Appl. Math. Mech. -Engl. Ed., **34**(6), 687–702 (2013)
DOI 10.1007/s10483-013-1700-7

Applied Mathematics and Mechanics (English Edition)

Conduction-radiation effect on natural convection flow in fluid-saturated non-Darcy porous medium enclosed by non-isothermal walls*

M. A. HOSSAIN[1], M. SALEEM[1], S. C. SAHA[2], A. NAKAYAMA[3]

(1. Department of Mathematics, COMSATS Institute of Information Technology, Park Road, Chak Shahzad, Islamabad 44000, Pakistan;
2. School of Chemistry, Physics & Mechanical Engineering, Queensland University of Technology, Brisbane 4000, Australia;
3. Department of Mechanical Engineering, Shizuoka University, Hamamatsu 422-8529, Japan)

Abstract The combined effect of conduction-convection-radiation on natural convection flow of an optically thick Newtonian fluid with gray radiant properties, confined in a porous media square cavity with Darcy-Brinkman-Forchheimer drag is studied numerically. For a gray fluid, Rosseland diffusion approximation is considered. It is assumed that (i) the temperature of the left vertical wall varies linearly with height, (ii) the right vertical and top walls are at a lower temperature, and (iii) the bottom wall is uniformly-heated. The governing equations are solved using the alternate direct implicit method together with the successive over relaxation technique. The investigation of the effect of governing parameters, namely, the Forschheimer resistance (Γ), the temperature difference (Δ), and the Plank number (Rd), on the flow pattern and heat transfer characteristics is carried out. It can be seen that the reduction of flow and heat transfer occur as the Forschheimer resistance is increased. On the other hand, both the flow strength and heat transfer increase as the temperature ratio Δ is increased.

Key words conduction-convection-radiation, Darcy-Brinkman-Forchheimer drag, porous medium, enclosure

Chinese Library Classification O361.3
2010 Mathematics Subject Classification 76W05

Nomenclature

a_{R},	the mean absorption coefficient;	g,	acceleration due to gravity;
$\boldsymbol{V}$,	velocity vector in two dimension;	Pr,	Prandtl number;
Da,	Darcy drag parameter;	q_{w},	dimensionless heat transfer rate;
x, y,	dimensional Cartesian coordinates;	$\boldsymbol{q}_{\mathrm{r}}$,	radiative flux vector;
F,	Forschheimer constant;	Ra,	Rayleigh number for thermal diffusion;
X, Y,	dimensionless Cartesian coordinates;	Rd,	Plank number;
K,	permeability of the porous media;	T,	temperature of the fluid in the boundary layer;
k,	thermal conductivity;		
k_{r},	radiative conductivity;	T_{H},	temperature at the heated surface;

* Received Sept. 26, 2012 / Revised Dec. 10, 2012
Corresponding author M. A. HOSSAIN, Professor, E-mail: anwar@univdhaka.edu

T_0, temperature of the cold surface;
U, V, dimensionless fluid velocities in the X- and Y-directions, respectively;
t, time;
c_p, Molar specific heat at constant pressure;
u, v, dimensional fluid velocities in the x- and y-directions, respectively.

Greek symbols

α, thermal diffusivity;
β, coefficient of thermal expansion;
Γ, Forschheimer resistance;
Δ, temperature ratio;
ρ, density of the fluid;
ν, kinematic viscosity;
σ, Stefan-Boltzman constant;
τ, dimensionless time;
ψ, stream function;
Ψ, dimensionless stream function;
ω, vorticity function;
θ, dimensionless temperature;
γ, porosity parameter;
Ω, dimensionless vorticity function.

1 Introduction

During the last three decades, a wide range of studies are conducted on conjugate heat transfer phenomena in porous media. It is of practical importance in a number of applications, for example, high performance insulation for buildings and cold storage installations. Nield and Bejan[1] presented an extensive review of existing studies on such topics. Reviews can also be found in Ingham and Pop[2], Pop and Ingham[3], Vafai[4], and Al-Amiri[5]. Numerical investigations of non-Darcian effects on transient conjugate natural convection-conduction heat transfer from a two-dimensional vertical plate fin embedded in a high-porosity medium were carried out by Hung et al.[6]. The results showed that the inertial effects on heat transfer characteristics are negligible at the beginning. However, these effects become increasingly important over longer periods of time. Furthermore, the two-dimensional transient conjugate free convection was investigated analytically and numerically by Vynnycky and Kimura[7] and Kimura et al.[8] using vertical plate in a porous medium.

Sen[9] considered Darcy-Brinkman convective flow in a shallow porous rectangular cavity with adiabatic upper and lower plate boundaries and differentially heated sidewalls. An important non-Darcian study has also been presented by Lauriat and Prasad[10] for a heated vertical porous cavity. The inertia and viscous forces on natural convection were examined via the Darcy-Brinkman-Forchheimer model. A numerical investigation of transient free convection in a two-dimensional square cavity filled with a porous medium was conducted by Saeid and Pop[11]. These results are in good agreement with the results obtained by Walker and Homsy[12], Bejan[13], Weber[14], Gross et al.[15], and Manole and Lage[16]. Also, the results show that the time required to reach steady state is shorter for high Rayleigh number and longer for low Rayleigh number. Finally, the classical Darcy formulation as well as the Darcy-Brinkman model, Darcy-Forchheimer model, and Darcy-Brinkman-Forchheimer model, has thoroughly been reviewed by Nield and Bejan[1].

It is worth mentioned that heat transfer in fluids which absorb and emit radiant energy is a task complicated by the coupled, non1linear physical phenomena of internal radiation (see Viskant and Anderson[17]) and natural convection (see Bejan[13]). There are several specific problems of scientific and technological interest in which heat transfer via radiation and convection occurs in optically thick liquids, such as the flow of the earth's mantle (see Matyska et al.[18]), the flow of oxide melts during crystal growth (see Rosenberger[19]), and the processing of molten glass (see Gardon[20]). In general, the interaction of radiant heat transfer and natural convection in finite enclosures has received considerable attention. Lauriat[21] analyzed the effect of combined radiation-convection in gray fluids flow enclosed in vertical cavities. Studies on natural convection of a participating fluid in a rectangular cavity heated by incident radiant energy through a transparent side wall were performed by Webb and Viskanta[22]. Fusegi

and Farouk[23] studied the laminar and turbulent natural convection-radiation interactions in a square enclosure filled with a non-gray gas for a wide range of Grashof number and Prandtl number. Yücel et al.[24] and Tan and Howell[25] investigated the flow of an absorbing, emitting, and scattering fluid in a differentially heated square enclosure. Salinger et al.[26] studied the effects of optical thickness and thermal gradients on the stability and structure of flows in a cylindrical container heated from below. Debry et al.[27] examined the performance of the approximations for modeling a representative problem of heat transfer and buoyant flow in optically thick fluids considering Rosseland diffusion approximation (also known as P1). This approximation is not applicable when the fluid is optically thin medium (see Siegel and Howell[28]). Recently, Gerardin et al.[29] modified this diffusion approximation and applied for simulation of radiative transfer in a 3D geometry for an absorbing scattering medium.

Here, we propose to investigate the natural convection flow of an optically thick radiative fluid saturated porous media confined in a square cavity. To see the effect of radiation here assume the Rosseland diffusion approximation. In order to account for the viscous and inertial effects in the momentum equation, the medium is considered to be porous due to Darcy-Brinkman-Forchheimer drag. Finally, we assume that the temperature of left vertical wall varies linearly with height, right vertical and top walls are cooled, and the bottom wall is uniformly-heated. This has importance for applications in developing technology and industry, such as prevention of sub-oil water pollution, storage of nuclear waste, and geothermal energy systems (for which Cheng[30] has provided an extensive review).

2 Mathematical formulation

The problem under investigation is a laminar, two dimensional natural convection flow of an optically thick fluid with Rosseland diffusion approximation in a cavity filled with saturated porous medium with Darcy-Brinkman-Forchheimer drag to account for the viscous and inertia effects in the momentum equation. The thermophysical properties of the fluid are assumed to be constant, except for the density in the buoyancy term of the momentum equations. Furthermore, the porous medium is considered homogeneous, isotropic, and saturated with a fluid that is in local thermodynamic equilibrium with the solid matrix of the porous medium. The physical system considered in the present investigation is illustrated in Fig. 1. The bottom wall of the enclosure is isothermal and maintained at T_{H}. The right and the top walls are maintained at a constant cold temperature T_0, such that $T_{\mathrm{H}} > T_0$. The temperature of the left wall is $(T_{\mathrm{H}} - T_0)(1 - y/H) + T_0$ so that it starts at temperature of the bottom and then reduces linearly to the temperature T_0 towards the top. The boundary condition at the right bottom corner deserves some explanation. In the reactor on which this model is based, a small gap of height H (5–10 mm) between the bottom and the right walls is filled with a sodium deposit. The temperature in the gap is expected to vary linearly from T_{H} to T_0 over a small distance L, as in the case of left wall (see Hossain and Wilson[31] and Saha and Gu[32] for triangular cavity problem).

Under the above assumptions, the continuity, momentum, and energy equations that govern the flow can be written as follows:

$$\frac{\partial u}{\partial x} + \frac{\partial v}{\partial y} = 0, \tag{1}$$

$$\frac{\partial u}{\partial t} + u\frac{\partial u}{\partial x} + v\frac{\partial u}{\partial y} = -\frac{1}{\rho}\frac{\partial p}{\partial x} + \nu\nabla^2 u - \frac{\nu\epsilon}{K}u - \frac{F\epsilon^2}{\sqrt{K}}|V|u, \tag{2}$$

$$\frac{\partial v}{\partial t} + u\frac{\partial v}{\partial x} + v\frac{\partial v}{\partial y} = -\frac{1}{\rho}\frac{\partial p}{\partial y} + \nu\nabla^2 v - \frac{\nu\epsilon}{K}v - \frac{F\epsilon^2}{\sqrt{K}}|V|v + g\beta(T - T_0), \tag{3}$$

$$\rho c_p\Big(\frac{\partial T}{\partial t} + u\frac{\partial T}{\partial x} + v\frac{\partial T}{\partial y}\Big) = k\nabla^2 T - \nabla\cdot\boldsymbol{q}_{\mathrm{r}}, \tag{4}$$

where F is the empirical constant in the second order resistance, β is thermal expansion coefficient, ρ is the density, μ is the dynamic viscosity, $\alpha = \frac{k}{\rho c_p}$ is thermal diffusivity in which c_p is Molar specific heat at constant pressure, k is the coefficient of thermal conductivity, and t is the time. In equation (4), $\nabla \cdot \boldsymbol{q}_\mathrm{r}$ is the divergence of the radiant flux vector represents the contribution of internal radiant transfer to the energy balance.

In equations (2) and (3), K is the measure of permeability of the porous medium (a packed bed of spheres), defined by

$$K = \frac{\epsilon^3}{180(1-\epsilon)^2} d^2,$$

where d is the diameter of the solid sphere, and ϵ is known as the porosity of the media and defined by

$$\epsilon = \frac{V_\mathrm{f}}{V_\mathrm{c}}.$$

Here, V_f is the volume of the fluid, and V_c is the control volume.

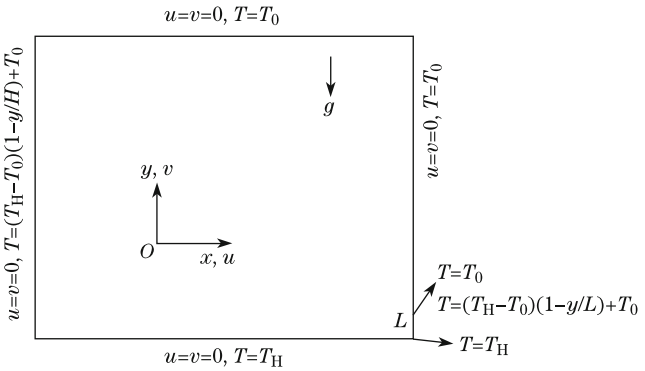

Fig. 1 Flow configuration and coordinate system

In the energy equation (4), $\boldsymbol{q}_\mathrm{r}$ is the diffusion heat flux for radiative heat transfer, which has the same form as that of the Fourier conduction law. Using the Rosseland mean absorption coefficient defined by Siegel and Howell[28], radiative flux vector can be written as

$$\boldsymbol{q}_\mathrm{r} = -k_\mathrm{r} \nabla T, \tag{5}$$

where k_r is the radiative conductivity defined by

$$k_\mathrm{r} = \frac{16\sigma T^3}{3a_\mathrm{R}}, \tag{6}$$

where σ and a_R are the Stefan-Boltzmann constant and the mean absorption coefficient, respectively. The energy equation together with equation (5) can be written as

$$\rho c_p \Big(\frac{\partial T}{\partial t} + u \frac{\partial T}{\partial x} + v \frac{\partial T}{\partial y} \Big) = k \nabla^2 T + \nabla \cdot (k_\mathrm{r} \nabla T). \tag{7}$$

Here, it is worth mentioned that Hossain and Wilson[31] investigated the problem of an enclosure filled with a fluid-saturated porous medium, along with generation of heat depending on the fluid temperature, but without effect of Forchheimer drag and internal radiation. On the other hand, Derby et al.[27] studied the buoyant flow of an optically thick fluid representative of

molten glass or an oxide crystal melt is solved the governing equations using the finite element method. They considered four different radiation models, namely, the Rosseland diffusion approximation with and without the radiation of slip, the P1, the approximation, and a rigorous numerical treatment, considering that the container top and bottom are cool and isothermal and that the side-wall is heated with a parabolic temperature distribution.

The solution procedure discussed here is based on equations involving ψ

$$u = \frac{\partial \psi}{\partial y}, \quad v = -\frac{\partial \psi}{\partial x}, \tag{8}$$

and the vorticity function ω,

$$\omega = \frac{\partial v}{\partial x} - \frac{\partial u}{\partial y}. \tag{9}$$

The vorticity equation obtained by eliminating the pressure between the momentum equations is given as below:

$$\begin{aligned} &\frac{\partial \omega}{\partial t} + u\frac{\partial \omega}{\partial x} + v\frac{\partial \omega}{\partial y} \\ &= \nu \nabla^2 \omega - \frac{\nu \epsilon}{K}\omega - \frac{F\epsilon^2}{\sqrt{K}}\Big(\frac{\partial(|V|v)}{\partial x} - \frac{\partial(|V|u)}{\partial y}\Big) + g\beta\frac{\partial T}{\partial x}. \end{aligned} \tag{10}$$

Now taking H as the reference length, and T_0 the temperature of the undisturbed fluid in the cavity as the reference temperature, we consider the following dimensionless dependent and independent variables

$$\begin{cases} X = \dfrac{x}{H}, \quad Y = \dfrac{y}{H}, \quad \tau = \dfrac{\nu}{H^2}t, \\ U = \dfrac{H}{\nu}u, \quad V = \dfrac{H}{\nu}v, \quad \Psi = \dfrac{\psi}{\nu}, \\ \Omega = \dfrac{\omega H^2}{\nu}, \quad \Theta = \dfrac{T - T_0}{T_{\mathrm{H}} - T_0}. \end{cases} \tag{11}$$

Using the above dimensionless variables in vorticity equation (10) and the energy equation (7), one may get the following dimensionless equations:

$$\begin{aligned} \frac{\partial \Omega}{\partial \tau} + U\frac{\partial \Omega}{\partial X} + V\frac{\partial \Omega}{\partial Y} &= \nabla^2 \Omega - (\gamma + \Gamma|\boldsymbol{V}|)\Omega \\ &\quad - \Gamma\Big(V\frac{\partial |\boldsymbol{V}|}{\partial X} - U\frac{\partial |\boldsymbol{V}|}{\partial Y}\Big) + \frac{Ra}{Pr}\frac{\partial \Theta}{\partial X}, \end{aligned} \tag{12}$$

$$\begin{aligned} \frac{\partial \Theta}{\partial \tau} + U\frac{\partial \Theta}{\partial X} + V\frac{\partial \Theta}{\partial Y} &= \frac{1}{Pr}\Big(1 + \frac{4}{3}Rd(1 + \Delta\Theta)^3\Big)\nabla^2\Theta \\ &\quad + \frac{4}{Pr}\Delta Rd(1 + \Delta\Theta)^2\Big(\Big(\frac{\partial \Theta}{\partial X}\Big)^2 + \Big(\frac{\partial \Theta}{\partial Y}\Big)^2\Big). \end{aligned} \tag{13}$$

From vorticity function given in equation (9), we get

$$\nabla^2 \Psi = -\Omega. \tag{14}$$

In a similar manner, from equation (8), we find the non-dimensional form of the velocity components

$$U = \frac{\partial \Psi}{\partial Y}, \quad V = -\frac{\partial \Psi}{\partial X}. \tag{15}$$

In the above equations

$$\begin{cases} Ra = \dfrac{g\beta(T_H - T_0)H^3}{\alpha\nu}, \quad Pr = \dfrac{\nu}{\alpha}, \\ \gamma = \dfrac{H^2}{K} = \dfrac{1}{Da}, \quad \Gamma = \dfrac{F\epsilon^2 H}{\sqrt{K}}, \\ Rd = \dfrac{4\sigma T_0^3}{ka_{\mathrm{R}}}, \quad \Delta = \dfrac{T_{\mathrm{H}} - T_0}{T_0}. \end{cases} \tag{16}$$

The physical significances of these parameters are listed as follows:

(a) the relative buoyancy potential given by the Rayleigh number Ra,

(b) the relative significance of the inertia term given by the Prandtl number Pr,

(c) the first-order rigid matrix resistance given by the porous media shape parameter γ, which is the ratio of the large length scale (taken to be the curvature instead of the gap spacing) to small length scale,

(d) second-order rigid matrix resistance or the Forchheimer drag coefficient given by Γ,

(e) the Plank number Rd,

(f) the temperature ratio Δ.

The boundary conditions imposed on the flow field are taken as (see Hossain and Wilson[31])

$$U = V = \Theta = 0$$

for $\tau = 0$. When $\tau > 0$,

$$\begin{cases} U = V = 0 \quad \text{for} \quad 0 \leqslant Y \leqslant 1 \quad \text{at} \quad X = 0, \\ U = V = \theta = 0 \quad \text{for} \quad 0 \leqslant X \leqslant 1 \quad \text{at} \quad Y = 1, \\ U = V = 0, \quad \Theta = 1 \quad \text{for} \quad 0 \leqslant X \leqslant 1 \quad \text{at} \quad Y = 0, \\ \Theta = 1 - Y \quad \text{for} \quad 0 \leqslant Y \leqslant 1 \quad \text{at} \quad X = 0, \\ \Theta = 1 - Y/A \quad \text{for} \quad 0 \leqslant Y \leqslant A \quad \text{at} \quad X = 1, \\ \Theta = 0 \quad \text{for} \quad A \leqslant Y \leqslant 1 \quad \text{at} \quad X = 1, \end{cases} \tag{17}$$

where

$$A = \frac{L}{H} = \frac{1}{10}.$$

Now, it is clear that for the present model, the non-dimensional parameters of interest are the Rayleigh number Ra, the Prandtl number Pr, the porosity parameter γ $(1/Da)$, the Forschheimer drag coefficient Γ, the Plank constant Rd, and the temperature ratio Δ. In the present investigation, pertaining to argon gas, the value of the Prandtl number is chosen as 0.7, and the Rayleigh number is taken to be 2×10^5.

3 Method of solution

For numerical simulation, here, successive over relaxation method with residual tolerance of order 10^{-5} is applied on the stream function equation (14). Considering H to be the reference height of the cavity, we take the uniform mesh size $h = H/j_{\max}$, where $j_{\max}$ is the maximum number of equi-spaced intervals along coordinate axes. The relaxation parameter r is obtained from the relation (see [33]), i.e.,

$$r = 2\Big(\frac{1 - \sqrt{(1 - \xi)}}{\xi}\Big), \tag{18}$$

where

$$\xi = \left(\frac{\cos\left(\frac{\pi}{j_{\max}-1}\right) + \cos\left(\frac{\pi}{j_{\max}-1}\right)}{2}\right)^2. \tag{19}$$

From these calculated values of stream function, the velocity components are updated using equation (12) at each time step. For transient vorticity transport and energy equations (15) and (16), we use alternate direct implicit (ADI) method. Given the values of variables Ω and θ in the flow field at any time step, we compute the values of Ω and θ at the next time step from equations (15) and (16). Forward time central space discretization is used for the transient and diffusion terms in the ADI method, whereas for the convective terms, the ADI method is modified using second upwind differencing technique. However, like other implicit methods, the stability requirement for vorticity at implicit wall boundaries imposes a restriction $\Delta\tau$ on the time step, in a form similar to that of explicit schemes. For uniform mesh size h, $\Delta\tau$ is given by (see [33])

$$\Delta\tau \leqslant \frac{1}{2\eta(\frac{2}{h^2}) + \frac{|u|+|v|}{h}}, \tag{20}$$

where η is the parameter that stands for the coefficient of diffusion term of the transport equations, whose solutions are required (see [33]). However, at solid wall boundaries, the time step restriction reduces to

$$\Delta\tau \leqslant \frac{h^2}{4\eta}. \tag{21}$$

Since the Prandtl number is fixed to be 0.7, thus for grid size of 71×71, equation (21) requires that a time step of $\Delta\tau = 10^{-6}$ would be appropriate for the entire computation in the proposed method. The computations, to reach to the steady state, are carried out till

$$\left|\frac{\theta^{m+1}_{(i,j)} - \theta^{m}_{(i,j)}}{\theta^{m}_{(i,j)}}\right| < 10^{-8}$$

is satisfied. Here, the superscript $'m'$ refers to the number of time step and (i, j) are spatial grid locations along X- and Y-axis, respectively. It is numerically testified that the steady state regime for all flow variables lies well within this range.

As before, like in Hossain and Wilson[31], a grid dependence study has been carried out for the present thermally-driven cavity flow taking Rd =1.0, 2.0, and 4.0 while Δ =0.5, $Da = 1\,000$, $\Gamma = 1.0$, $Pr = 0.7$, and $Ra = 2 \times 10^5$ with meshes of 41×41, 55×55, 61×61, and 71×71 points. Thus, the numerical values obtained for $\psi_{\min}$ and $\psi_{\max}$ are entered in Table 1. Finally, for computational economy, a 61×61 mesh is used throughout the present simulations.

Table 1 Numerical values of $\psi_{\min}$ and $\psi_{\max}$ for $Rd = 1.0$, 2.0, and 4.0 while $\Delta = 0.5$, $Da = 1\,000$, $\Gamma = 1.0$, $Pr = 0.7$, and $Ra = 2 \times 10^5$

Rd	41×41		55×55		61×61		71×71	
	$\psi_{\min}$	$\psi_{\max}$	$\psi_{\min}$	$\psi_{\max}$	$\psi_{\min}$	$\psi_{\max}$	$\psi_{\min}$	$\psi_{\max}$
1.0	–15.382	1.303 5	–15.431	1.356 7	–15.430	1.347 6	–15.402	1.336 6
2.0	–14.203	0.969 1	–14.195	0.961 2	–14.196	0.960 2	–14.188	0.951 9
4.0	–12.378	0.284 4	–12.362	0.264 1	–12.358	0.262 5	–12.345	0.250 8

The corresponding problem on natural convection flow in a fluid-saturated porous medium enclosed by non-isothermal walls but without the effect of radiation ($Rd = 0$) and Forschheimer

drag ($\Gamma = 0$) was investigated by Hossain and Wilson[31] for $Pr = 0.7$ and $\gamma = 10$. However, knowing the temperature distribution, we can evaluate the net radiative heat flux in the medium. However, the limitation to the accuracy of the optically thick limit approximation should be recognized. According to Ozisik[34], this approximation breaks down in the intermediate vicinity of the boundaries because it does not take into account radiation from the boundary surface. This is a serious restriction, since heat transfer at the wall is important. Thus, with black body condition for optically thick limit the net wall heat flux forms the following relations:

$$\begin{cases} q_{\mathrm{L}} = -\Big(1 + \dfrac{2}{3} Rd(1 + \Delta\theta|_{X=0})^3\Big)\Big(\dfrac{\partial\theta}{\partial X}\Big)_{X=0}, \\ q_{\mathrm{R}} = \Big(1 + \dfrac{2}{3} Rd(1 + \Delta\theta|_{X=1})^3\Big)\Big(\dfrac{\partial\theta}{\partial X}\Big)_{X=1}, \\ q_{\mathrm{B}} = -\Big(1 + \dfrac{2}{3} Rd(1 + \Delta\theta|_{Y=0})^3\Big)\Big(\dfrac{\partial\theta}{\partial Y}\Big)_{Y=0}, \\ q_{\mathrm{T}} = \Big(1 + \dfrac{2}{3} Rd(1 + \Delta\theta|_{Y=1})^3\Big)\Big(\dfrac{\partial\theta}{\partial Y}\Big)_{Y=1}. \end{cases} \tag{22}$$

Here, q_{L}, q_{R}, q_{B}, and q_{T} are, respectively, the net heat flux from the left, right, bottom, and top surface of the cavity. It follows that the net average heat transfer corresponding to the above net heat transfer coefficients are calculated as

$$\begin{cases} Q_{\mathrm{L}} = \displaystyle\int_0^1 q_{\mathrm{L}} \mathrm{d}Y, \quad Q_{\mathrm{R}} = \int_0^1 q_{\mathrm{R}} \mathrm{d}Y, \\ Q_{\mathrm{B}} = \displaystyle\int_0^1 q_{\mathrm{B}} \mathrm{d}X, \quad Q_{\mathrm{T}} = \int_0^1 q_{\mathrm{T}} \mathrm{d}X, \end{cases} \tag{23}$$

where Q_{L}, Q_{R}, Q_{B}, and Q_{T} are, respectively, the net average heat flux from the left, right, bottom, and top surface of the cavity.

4 Results and discussion

We have considered the effect of surface radiation on natural convection flow in a rectangular porous enclosure filled with a Newtonian fluid. The temperature of the left vertical wall linearly reduces to zero from bottom to top, whereas the lower end of the right wall is subject to a steep temperature gradient. The results are presented in terms of streamlines, isotherms, and heat transfer rate of the walls for different values of the governing parameters.

4.1 Effect of Forschheimer resistance Γ

Since the pressure drop in Darcy-Forchheimerr model does not strictly vary linearly with the velocity components. That is, in addition to the usual viscous resistance of the Darcy model for low velocities, as it was in the case of Hossain and Wilson[31], the inertial acceleration/retardation also comes into account for higher velocities. Figure 2 shows the selected results of steady state pattern of streamlines at $Ra = 2 \times 10^5$, $Pr = 0.7$, $Rd = 0.0$, $\gamma = 1\,000$, and $\Delta = 0.5$ for (a) $\Gamma = 0.0$, (b) $\Gamma = 25.0$, and (c) $\Gamma = 50.0$, respectively. As can be seen by comparing Figs. (a), (b), and (c) in Fig. 2 that in the absence of radiation effects, the volume flow rate in both the primary and the secondary cells decreases with the increase in Γ. This reduction in the flow may well be attributed to an overall increase in the resistance to the flow due to combined viscous and inertial losses. However, despite the reduction of the flow, the flow pattern does not change considerably. Figure 3 now shows the isotherms at $Ra = 2 \times 10^5$, $Pr = 0.7$, $Rd = 0.0$, $\gamma = 1\,000$, and $\Delta = 0.5$ for (a) $\Gamma = 0.0$, (b) $\Gamma = 25.0$, and (c) $\Gamma = 50.0$, respectively. It can be seen from Fig. 3 that the isotherms seem to originate from the lower part of the right wall. This is the region where the temperature of the wall drops sharply to zero. That is the region of steep temperature gradient along the vertical. However, this cluster seems evenly distributed along the left wall, which is because of the imposed boundary conditions.

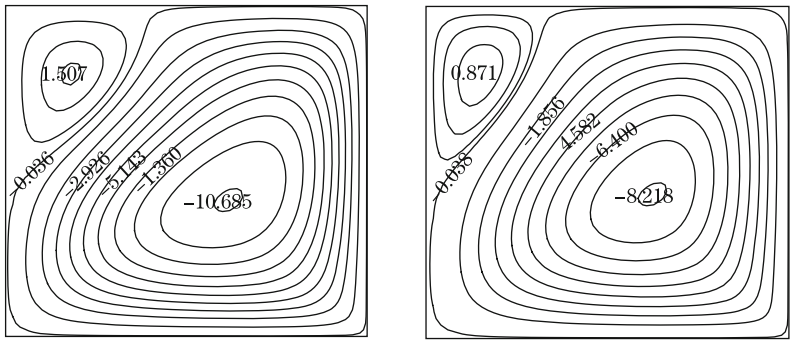

(a) Γ =0.0 (b) Γ =25.0

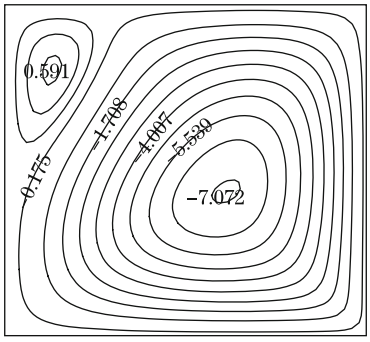

(c) Γ =50.0

Fig. 2 Streamlines for different Γ while $\gamma = 10^3$, Rd=0.0, $\Delta = 0.5$, $Pr = 0.7$, and $Ra = 2 \times 10^5$

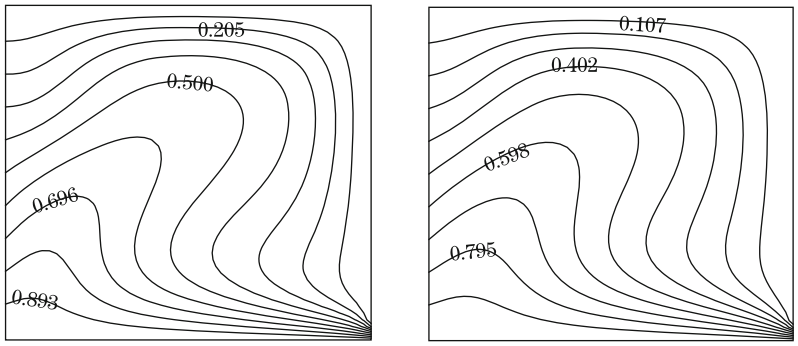

(a) Γ =0.0 (b) Γ =25.0

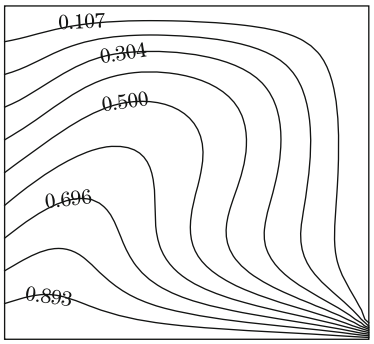

(c) Γ =50.0

Fig. 3 Isotherms for different Γ while $\gamma = 10^3$, Rd=0.0, $\Delta = 0.5$, $Pr = 0.7$, and $Ra = 2 \times 10^5$

The labeled contours of isotherms also depict how the temperature is distributed along the vertical wall. It can be seen that the pattern of temperature distribution is not much affected due to the increasing effect of the Forchheimer resistance Γ.

Figures 4(a)–4(d) show the heat transfer rate of the solid walls at $Ra = 2 \times 10^5$, $Pr = 0.7$, $Rd = 0.0$, and $\gamma = 1\,000$ for different values of Γ. Figure 4(a) shows the heat transfer rate of the left wall. It can now be observed that for $\Gamma = 0$, a wave like structure of heat transfer curve appears. However, the distribution transforms to a single peak curve for $\Gamma = 50$. Moreover, this peak value decreases with the increase in the value of Γ. Thus, heat transfer along the left wall numerically decreases with the increase in the value of Γ. Figure 4(b) shows the heat flux distribution for the right wall. It can be seen that for all values of Γ, the heat transfer curve shoots down from its maximum value in the region $0 \leqslant Y \leqslant A$, which is the region of steep temperature variation along the right wall. However, the curves drop to the minimum close to $Y = 0.2$. The decrease in the local maximum of the curves in the region $0.2 \leqslant Y \leqslant 1$ show that the heat transfer rate decreases for increasing values of Γ. Figure 4(c) shows the heat transfer curves for the bottom wall. Comparing Figs. 4(a) and 4(c), we see that the heat flux distribution is different for left and bottom walls which may well be attributed to the imposed surface heating conditions. As the bottom wall is at a constant temperature and the heat transfer shoots to maximum close to $X = 1$, which may be due to the reason that $X = 1$ is the region of steep temperature difference along the right wall. This behaviour is due to the temperature conditions imposed along these walls. Figure 4(d) now shows the heat transfer rate of the top wall. For all values of Forschheimer resistance Γ, the heat flux is unity along the left and zero along the right end of the top wall due to the boundary conditions. In between, a peak value appears in each curve. This corresponds to the region where the fluid coming from

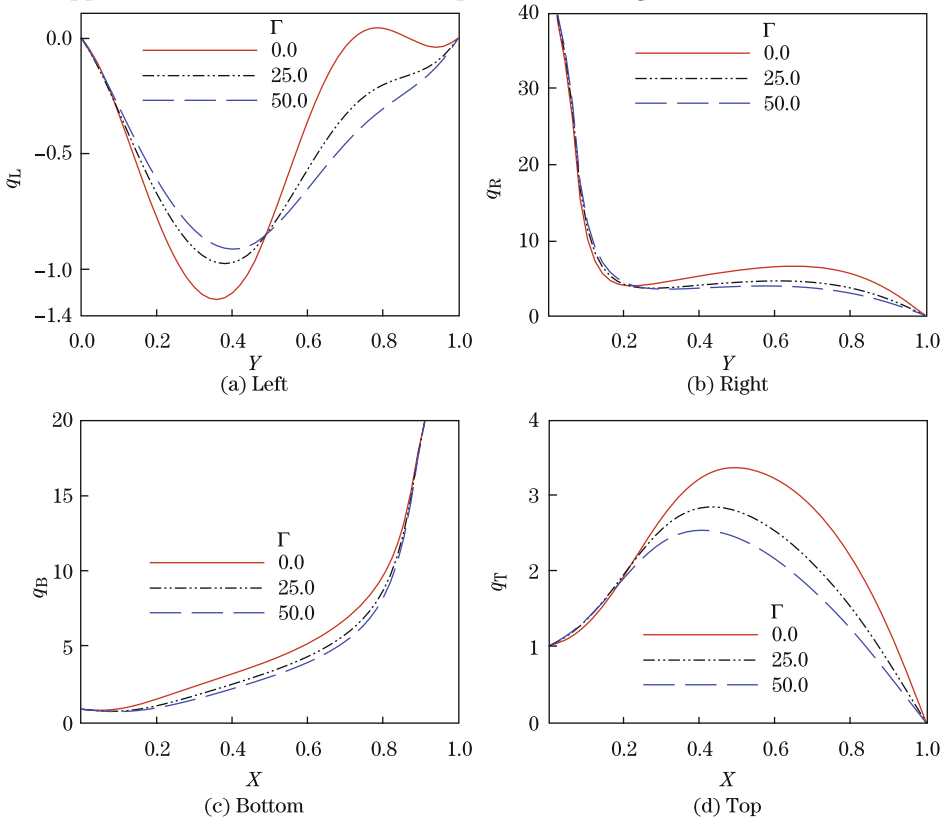

Fig. 4 Rate of heat transfer q_w from different walls for Γ =0.0, 25.0, and 50.0 while $\gamma = 10^3$, Rd=0.0, $\Delta = 0.5$, $Pr = 0.7$, and $Ra = 2 \times 10^5$

the left wall meets the top surface. However, like the other three walls, the decrease in this peak value shows that the heat transfer decreases with increasing values of Γ. Thus, from the above discussion, we conclude that the heat transfer rate for all the four walls decreases with the increase in the value of Forchheimer resistance, and it is due to decreased fluid motion as an effect of Γ.

4.2 Effect of surface temperature Δ

Figure 5 shows the pattern of streamlines at $Ra = 2 \times 10^5$, $Pr = 0.7$, and $\Gamma = Rd = 1.0$ for (a) $\Delta = 0.5$, (b) $\Delta = 1.0$, and (c) $\Delta = 1.5$, respectively. It can now be seen that with the increase in the value of Δ, the volume flow rate and the size of the primary cell increases. This is now expected since the increase in the value of Δ corresponds to an increase in the temperature distribution close to the walls at a higher temperature and/or alternatively a decrease in the temperature distribution of the fluid close to the walls at a lower temperature distribution. This makes sense why the strength of the secondary cell decreases for increasing values of Δ. Further, not only the size, but also the strength of flow in the primary cells increase from 0.56

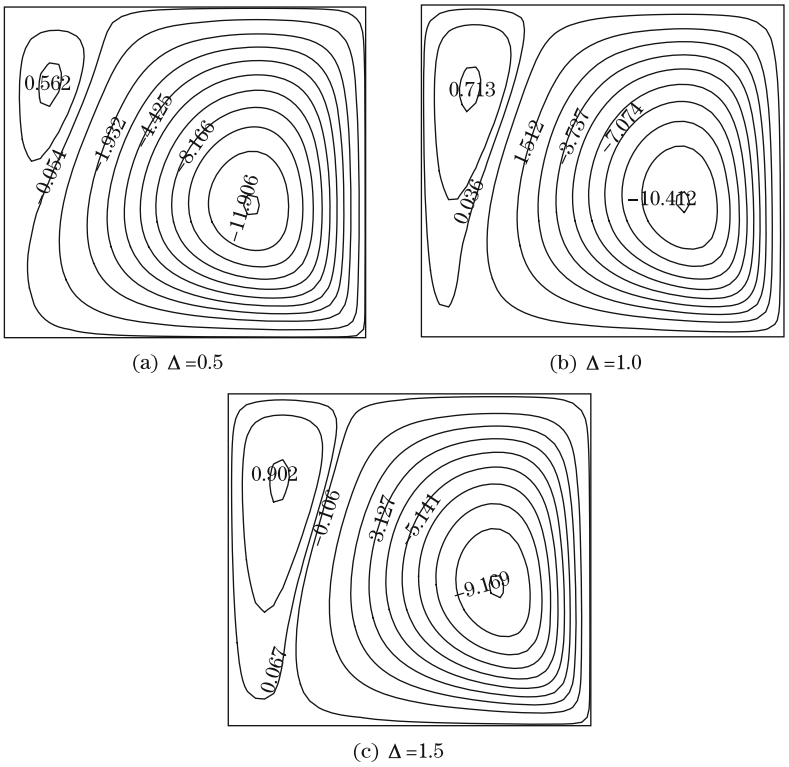

Fig. 5 Streamlines for different Δ while $\gamma = 10^3$, Γ =1, Rd=1.0, $Pr = 0.7$, and $Ra = 2 \times 10^5$

to 0.90 as Δ is increased from 0.5 to 1.5. Figure 6 shows isotherms at $Ra = 2\times10^5$, $Pr = 0.7$, and $\Gamma = Rd = 1.0$ for (a) $\Delta = 0.5$, (b) $\Delta = 1.0$, and (c) $\Delta = 1.5$, respectively. One can see that the the temperature distribution remains smoother, and does not vary significantly as Δ increases. This may be due to the reason that the flow pattern also does not change very significantly.

Since Δ corresponds to the temperature difference, we discern that an increase in Δ would increase the temperature difference between the walls. Figures 7(a)–7(d) now show the heat flux distribution of the left, right, bottom and top walls, respectively, at $Ra = 2\times10^5$, $Pr = 0.7$, $\Gamma = Rd = 1.0$, $\gamma = 1\,000$ for different values of Δ. Figure 7(a) shows the heat flux distribution of the left wall. From this figure, we now discern that the wave like structure that appeared in Fig. 4(a) for $\Gamma = Rd = 0$, does not appear for non-zero values of Γ and Rd. However, one peak

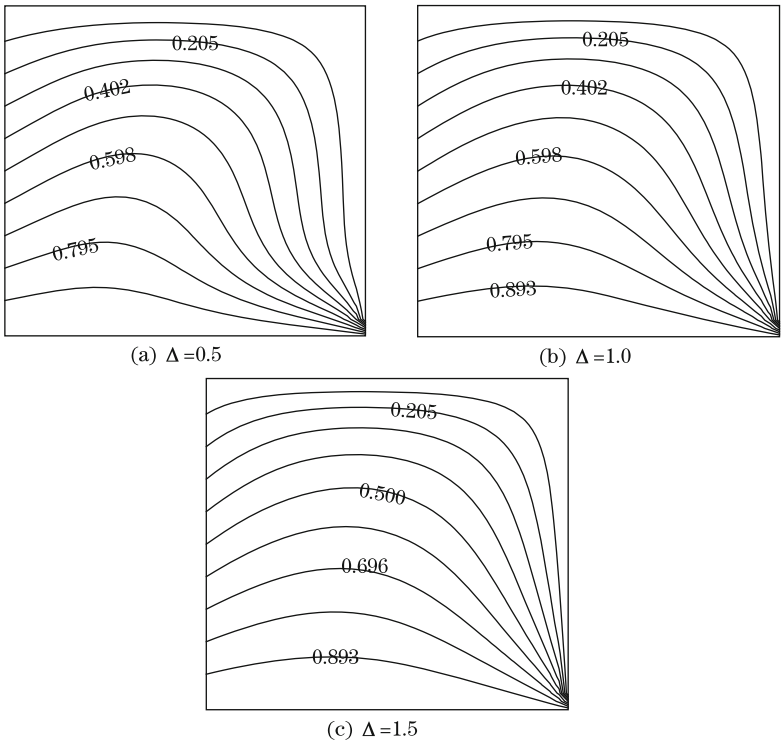

Fig. 6 Isotherms for different Δ while $\gamma = 10^3$, Γ =1, Rd=1.0, $Pr = 0.7$, and $Ra = 2 \times 10^5$

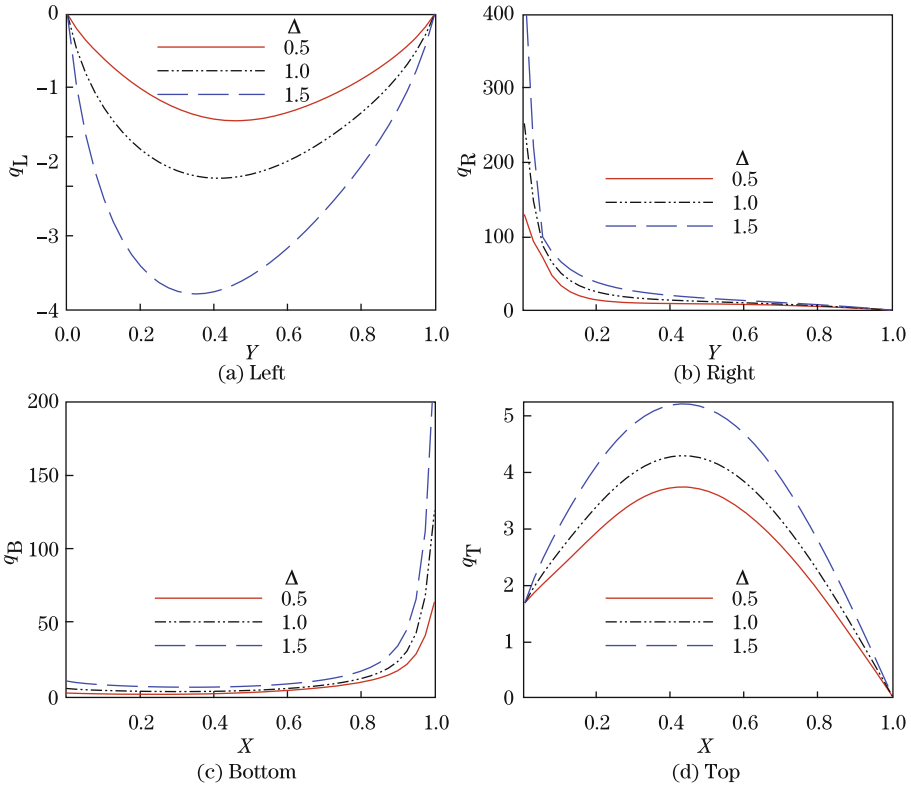

Fig. 7 Rate of heat transfer from different walls for Δ =0.5, 1.0, and 1.5 while $Rd = 1.0$, $\gamma = 10^3$, Γ =1.0. $Pr = 0.7$, and $Ra = 2 \times 10^5$

value appears which numerically increases for increasing values of Δ. Figure 7(b) shows the heat flux distribution of the right wall. It can now again be seen that the heat transfer drops to its minimum close to $Y = 0.2$. However, heat transfer slightly increases as Δ increases. This is now expected since an increase in Δ causes the temperature gradient along the lower part of the right wall also to increase. Nevertheless, unlike Fig. 4(b), this peak value in Fig. 7(b) asymptotically drops to zero in the range $0.2 \leqslant Y \leqslant 1$, showing that the heat transfer increases for increasing values of Δ. Figure 7(c) depicts the heat flux distribution of the bottom wall. It is now easy to understand that the heat flux distributions of the left wall reaches to its maximum close to $X = 1$ due to imposed boundary temperature around the right bottom. This maximum value also increases as Δ increases. Figure 7(d) finally represents the heat flux of the top wall, which shows that like other three walls, the heat transfer rate of the right wall also increases as Δ increases. However, comparing it with Fig. 4(d), we see that its value at $X = 0$ is not unity, rather it is 1.7 which is due to non-zero value of Rd, that makes contribution in heat transfer given by equations (22). Also, the heat flux in this case is greater than the one in the case of $Rd = 0$ given in Fig. 4(d).

4.3 Effect of Plank number *Rd*

Figures 8 and 9 respectively show the streamlines and isotherms at $Ra = 2 \times 10^5$, $Pr = 0.7$, $\Gamma = 1.0$, $\gamma = 10^3$, $\Delta = 0.5$ for (a) $Rd = 0.0$, (b) $Rd = 2.0$, and (c) $Rd = 4.0$. Figures 8(a)–8(c) reveal that there is an overall decrease in the strength of flow both in primary and secondary cells, with the increase in the value of Rd. Moreover, the transition of flow from two cell to one cell pattern also suggests that the contribution of Rd causes a reduction in the convective flow. The increase in the radiation effects may enhance the fluid temperature, which ultimately reduces the temperature difference between the walls and the ambient fluid, thereby reducing the overall flow rate. Figures 9(a)–9(c) indicate that the temperature distribution in the flow region is not much affected by the variation of Rd.

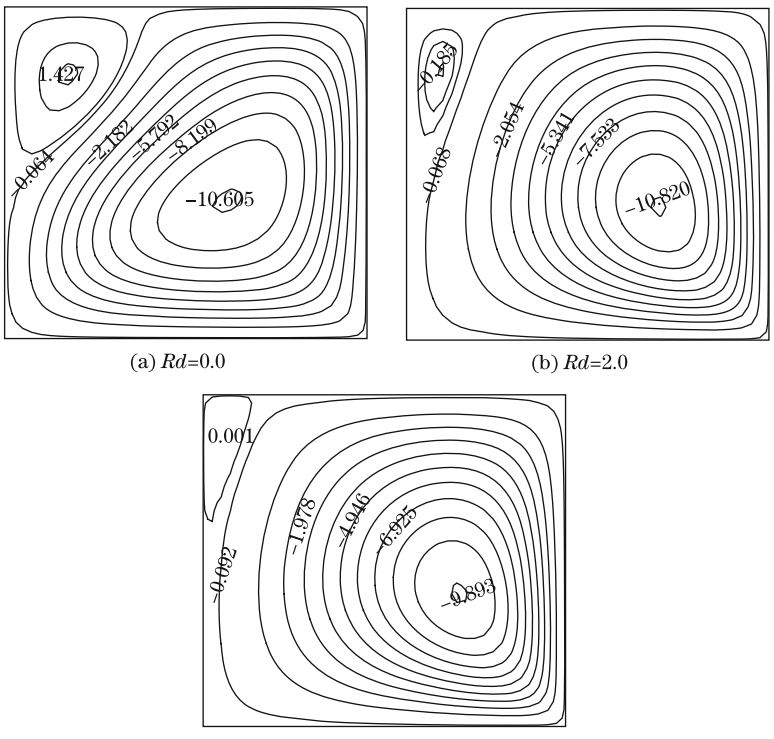

(a) Rd=0.0 (b) Rd=2.0

(c) Rd=4.0

Fig. 8 Streamlines for different Rd while Δ =0.5, $\gamma = 10^3$, Γ=1.0, $Pr = 0.7$, and $Ra = 2 \times 10^5$

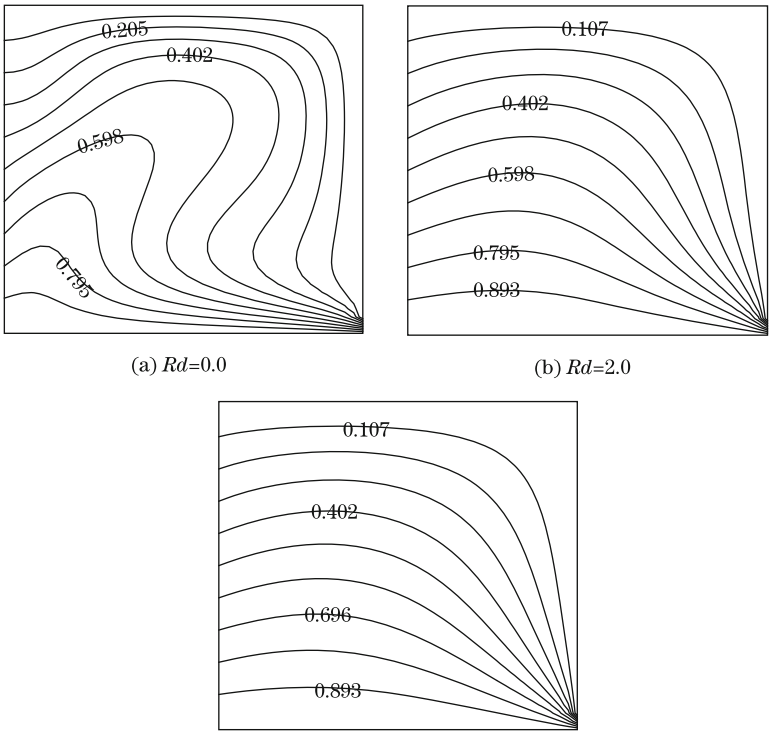

(a) Rd=0.0 (b) Rd=2.0

(c) Rd=4.0

Fig. 9 Isotherms for different Rd while $\Delta = 0.5$, $\gamma = 10^3$, $\Gamma = 1.0$, $Pr = 0.7$, and $Ra = 2 \times 10^5$

The consideration of black body conditions in optically thick limits of solid walls leads to a heat transfer characteristics, which is also complemented with the effect of Rd. This net/enhanced heat transfer rate with the added effect of Rd is defined in equations (22). Figure 10 represents the heat flux distributions of the (a) left, (b) right, (c) bottom, and (d) top solid walls at $Ra = 2 \times 10^5$, $Pr = 0.7$, $\gamma = 10^3$, $\Gamma = 1.0$, $\Delta = 0.5$, for $Rd = 0.0, 2.0$, and 4.0, respectively. It is now clear from these figures that the heat transfer rate of the four walls increases with the increase in Rd. However, Fig. 10(d) needs some attention. The heat flux distribution at the left end top is unity for $Rd = 0$, but it increases for non zero values of Rd. This is due to the enhanced effect of Rd on the heat flux.

5 Conclusions

We considered the radiation effect on natural convection flow in a fluid-saturated porous medium in a rectangular enclosure, with temperature gradient subject to the non-isothermal walls. The temperature of the left wall varies linearly, whereas the lower end of the right wall also reduces to zero within 1/10th of its height. The results reveal that the flow reduces with the increase in Forschheimer resistance Γ and the Plank number Rd. However, the strength of the vortex in the vicinity of the non-isothermal wall increases with the increase in the value of temperature difference Δ. The heat transfer rate of the solid walls decreases with the increase in this Forschheimer resistance Γ, whereas it increases for increasing values of the temperature difference Δ and the Plank number Rd. However, this increasing/decreasing trend in heat transfer is more pronounced for Δ and Rd.

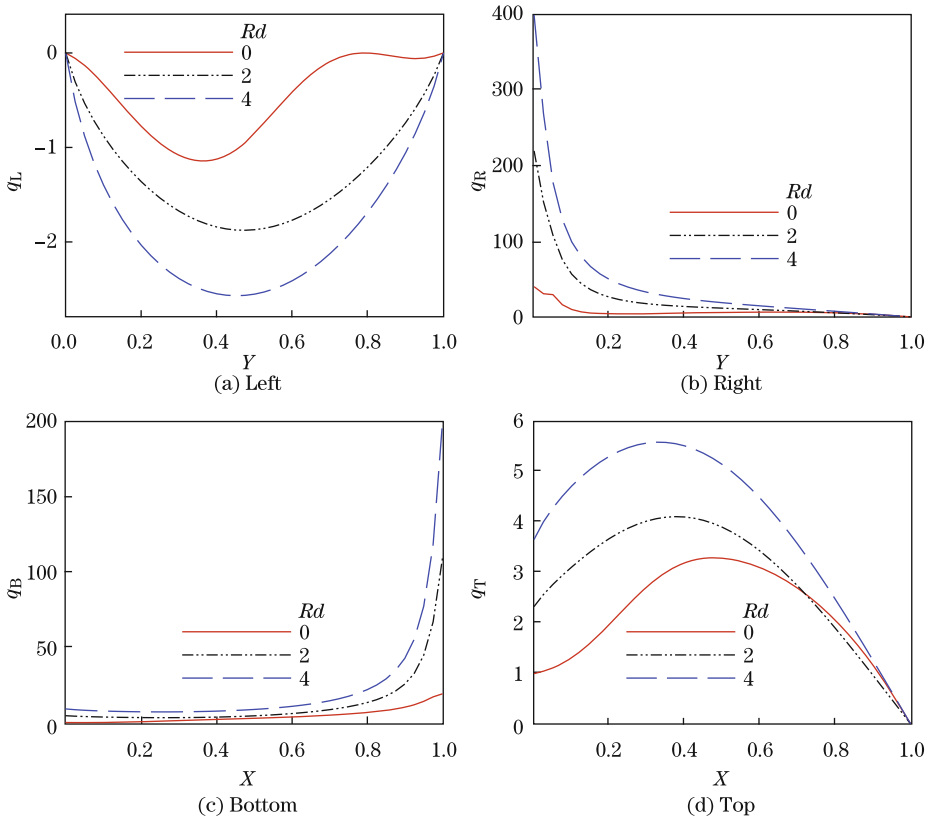

Fig. 10 Rate of heat transfer from different walls for Rd =0.0, 2.0, and 4.0 while $\Delta = 0.5$, $\gamma = 10^3$, γ =1.0, $Pr = 0.7$, and $Ra = 2 \times 10^5$

References

[1] Nield, D. A. and Bejan, A. *Convection in Porous Media*, 3rd ed., Springer Science + Business Media, New York (2006)

[2] Ingham, D. B. and Pop, I. *Transport Phenomenon in Porous Media*, Pergamon, Oxford (1998)

[3] Pop, I. and Ingham, D. B. *Convective Heat Transfer*: *Mathematical and Computational Modeling of Viscous Fluids and Porous Media*, Pergamon, Oxford (2001)

[4] Vafai, K. *Handbook of Porous Media*, 2nd ed., Taylor and Francis Group, New York (2005)

[5] Al-Amiri, A. Natural convection in porous enclosures: the application of the two-energy equation model. *Numerical Heat Transfer*: *Part A*, **41**, 817–834 (2002)

[6] Hung, C. I., Chen, C. O. K., and Cheng, P. Transient conjugate natural convection heat transfer along a vertical plate fin in a high-porosity medium. *Numerical Heat Transfer*: *Part A*, **15**, 133–148 (1989)

[7] Vynnycky, M. and Kimura, S. Transient conjugate free convection due to a vertical plate in a porous medium. *Int. J. Heat Mass Tran.*, **38**, 219–231 (1995)

[8] Kimura, S., Kiwata, T., and Okajima, A. Conjugate natural convection in porous media. *Advanced in Water Resources*, **20**, 111–126 (1997)

[9] Sen, A. K. Natural convection in a shallow porous cavity—the Brinkman model. *Int. J. Heat Mass Tran.*, **30**, 855–868 (1987)

[10] Lauriat, G. and Prasad, V. Non-Darcian effects on natural convection in a vertical porous enclosure. *Int. J. Heat Mass Tran.*, **32**, 2135–2148 (1989)

[11] Saeid, N. H. and Pop, I. Transient free convection in a square cavity filled with a porous medium. *Int. J. Heat Mass Tran.*, **47**, 1917–1924 (2004)

[12] Walker, K. L. and Homsy, G. M. Convection in a porous cavity. *J. Fluid Mech.*, **87**, 474–499 (1978)

[13] Bejan, A. *Convection Heat Transfer*, Wiley-Interscience, New York (1984)

[14] Weber, J. E. The boundary-layer regime for convection in a vertical porous layer. *Int. J. Heat Mass Tran.*, **18**, 569–573 (1975)

[15] Gross, R. J., Baer, M. R., and Hickox, C. E. Application of flux-corrected transport (FCT) to high Rayleigh number natural convection in a porous medium. *Proceedings of the International Heat Transfer Conference on Heat Transfer*, Lalifornia, San Francissco (1986)

[16] Manole, D. M. and Lage, J. L. Numerical benchmark results for natural convection in a porous medium cavity. *American Society of Mechanical Engineers*, **216**, 55–60 (1992)

[17] Viskanta, R. and Anderson, E. E. Heat transfer in semitransparent solids. *Advances in Heat Transfer*, Academic Press, New York (1975)

[18] Matyska, C., Moser, J., and Yuen, D. A. The potential influence of radiative ransfer on the formation of megaplumes in the lower mantle. *Earth and Planetary Science Letters*, **125**, 255–266 (1994)

[19] Rosenberger, F. E. *Fundamentals of Crystal Growth* I: *Macroscopic Equilibrium and Transport Concepts*, Springer-Verlag, Berlin (1979)

[20] Gardon, R. A review of radiant heat transfer in glass. *J. Am. Ceram. Soc.*, **44**, 305–312 (1961)

[21] Lauriat, G. Combined radiation-convection in gray fluids enclosed n vertical cavities. *Journal of Heat Transfer*, **104**, 609–615 (1982)

[22] Webb, B. W. and Viskanta, R. Analysis of radiation-induced natural convection in rectangluar enclosures. *Journal of Thermophysics*, **1**, 146–153 (1987)

[23] Fusegi, T. and Farouk, B. Laminar and turbulent natural convection diation interactions in a square enclosure filled with a nongray gas. *Numerical Heat Transfer*: *Part A*, **15**, 303–322 (1989)

[24] Yücel, A., Acharya, S., and Williams, M. L. Natural convection and radiation in square enclosures. *Numerical Heat Transfer*: *Part A*, **15**, 261–278 (1989)

[25] Tan, Z. and Howell, J. R. Combined radiation and natural convection in a two-dimensional participating square medium. *Int. J. Heat Mass Tran.*, **34**, 785–793 (1991)

[26] Salinger, A. G., Brandon, S., Aris, R., and Derby, J. J. Buoyancy-driven flows of a radiatively participating fluid in a vertical cylinder heated from below. *Proc. R. Soc. Lond. A*, **442**, 313–341 (1993)

[27] Derby, J. J., Brandon, S., and Salinger, A. G. The diffusion and P1 approximations for modeling buoyant flow of an optically thick fluid. *Int. J. Heat Mass Tran.*, **41**, 1405–1415 (1998)

[28] Siegel, R. and Howell, J. R. *Thermal Radiation Heat Transfer*, 2nd ed., McGraw-Hill, New York (1981)

[29] Gerardin, J., Seiler, N., Ruyer, P., Trovalet, L., and Boulet, P. P1 approximation, MDA and IDA for the simulation of radiative transfer in a 3D geometry for an absorbing scattering medium. *Journal of Quantitative Spectroscopy and Radiative Transfer*, **113**, 140–149 (2012)

[30] Cheng, P. Heat transfer in geothermal systems. *Advanced in Heat Transfer*, **4**, 1–105 (1978)

[31] Hossain, M. A. and Wilson, M. Natural convection flow in a fluid-saturated porous medium enclosed by non-isothermal walls with heat generation. *Int. J. Therm. Sci.*, **41**, 447–454 (2002)

[32] Saha, S. C. and Gu, Y. T. Free convection in a triangular enclosure with fluid-saturated porous medium and internal heat generation. *ANZIAM Journal*, **53**, C127–C141 (2011)

[33] Roache, P. J. *Computational Fluid Dynamics*, 2nd ed., Hermosa, Albuquerque, New Mexico (1998)

[34] Ozisik, M. N. *Radiative Transfer and Interactions with Conduction and Convection*, John-Wiley & Sons, New York (1973)